minerals

MDPI

Article

The Characteristics and Enrichment Process of Dabu Ion-Adsorption Heavy Rare-Earth Element (HREE) Deposits in Jiangxi Province, South China

Mingjun Xie [1,2], Jian Zhou [1,*], Xuemiao Du [1,*], Xueqiu Wang [1], Bimin Zhang [1], Hui Wu [1], Qinghai Hu [1], Wei Wang [1], Mi Tian [1], Binfeng Chen [3], Huohua Mo [3] and Lijun Wang [1]

[1] Institute of Geophysical and Geochemical Exploration, Chinese Academy of Geological Sciences, Langfang 065000, China; xmj111000@163.com (M.X.); wxueqiu@mail.cgs.gov.cn (X.W.); zbimin@hotmail.com (B.Z.); wuhui@igge.cn (H.W.); huqinghai0616@foxmail.com (Q.H.); wangwei@igge.cn (W.W.); tianmi@igge.cn (M.T.); wanglijun@igge.cn (L.W.)
[2] School of Earth Sciences and Resources, China University of Geosciences Beijing, Beijing 100083, China
[3] Geological Survey Team of Gannan, Bureau of Geology and Mineral Exploration and Development of Jiangxi Province, Ganzhou 341000, China; chenbinfen@163.com (B.C.); m18370982018@163.com (H.M.)
* Correspondence: zhoujian@mail.cgs.gov.cn (J.Z.); dxuemiao@mail.cgs.gov.cn (X.D.)

Abstract: Ion-adsorption rare-earth deposits supply over 90% of the global market's heavy rare-earth elements (HREEs). The genesis of these deposits, particularly HREE deposits, has garnered significant attention. To elucidate the metallogenic mechanisms of HREE deposits, a comprehensive study of the weathering profile of granite was conducted in Jiangxi Province, South China. This study focuses on the following two aspects: the petrogeochemistry of HREE-rich granite and the enrichment and fractionation of rare-earth elements (REEs) during the weathering process. The results suggest that the Dabu granites are a typical peraluminous, high-K, calc-alkaline granite series with high silica content (SiO_2: 74.5%–76.4%), relatively low phosphorus content (P_2O_5: <0.05%), and high HREE content (ΣLREE/ΣHREE: 0.16–0.66). Weathering advances the decomposition of minerals and the release of elements. REEs are mainly fixed in the regolith by scavengers, mainly clays, Fe–Mn oxides, and carbonates, and ΣREE can reach 799 ppm in the B horizon. However, HREEs tend to migrate further and preferentially combine with Fe–Mn oxides and carbonates as compared to LREEs, leading to a significant fractionation of REEs in the regolith (ΣLREE/ΣHREE = 0.2–1.1). Additionally, the differential weathering of REE-bearing minerals and the precipitation of secondary REE-bearing minerals are also vital for REE fractionation.

Keywords: petrogeochemistry; weathering process; REE fixation; REE fractionation; ion-adsorption-type REE deposit

Citation: Xie, M.; Zhou, J.; Du, X.; Wang, X.; Zhang, B.; Wu, H.; Hu, Q.; Wang, W.; Tian, M.; Chen, B.; et al. The Characteristics and Enrichment Process of Dabu Ion-Adsorption Heavy Rare-Earth Element (HREE) Deposits in Jiangxi Province, South China. *Minerals* **2024**, *14*, 857. https://doi.org/10.3390/min14090857

Academic Editor: Bernard Hubbard

Received: 29 June 2024
Revised: 10 August 2024
Accepted: 21 August 2024
Published: 24 August 2024

1. Introduction

Rare-earth elements (REEs), including the lanthanide group elements (La to Lu) along with Y and Sc, are recognized as strategic resources and critical metals, owing to their similar physical and chemical characteristics [1]. REEs are crucial for renewable energy and advanced technology applications [2–6]. Recently, the global demand for REEs, especially heavy REEs (HREEs: Gd to Lu and Y), has dramatically increased with the rapid development of emerging industries [7,8]. HREEs are predominantly found in ion-adsorption rare-earth deposits, which are formed by the weathering of granitoids. Statistics indicate that more than 170 ion-adsorption rare-earth deposits (IAREDs) have been discovered in South China. Although only 10% of these are predominantly composed of HREEs (Figure 1a,b), they still meet more than 90% of the global market demand for HREEs [9,10].

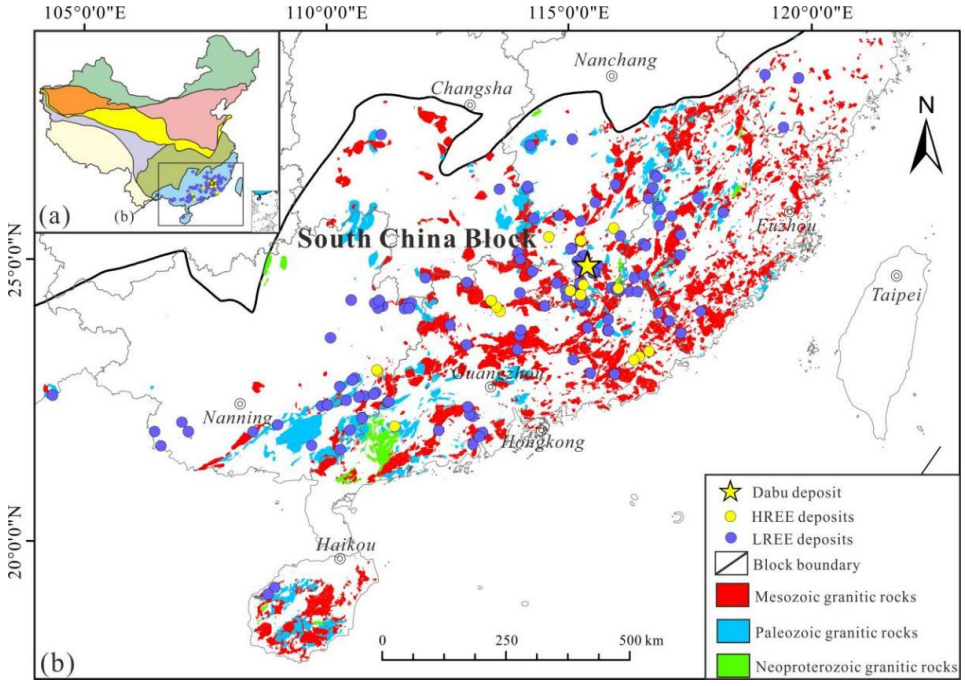

Figure 1. (**a**) Simplified tectonic map with ion-adsorption REE deposits in South China (modified by [11] and different colored areas represent different tectonic units of China); (**b**) Geological maps showing the distribution of granites and REE deposits in southern China (modified by 1:2,500,000 geological map of China), the yellow star represents the Dabu deposit.

Previous studies have suggested that various lithologies, such as granites, metamorphic rocks, volcanic rocks, and basic–ultrabasic rocks, can generate ion-adsorption LREE deposits [3,12–17]. However, HREE deposits can only be formed by the weathering of granites [4,6,10,12,15,18]. Moreover, the granites related to HREE deposits are usually distinct in rock type and geochemical characteristics compared with those associated with LREE deposits [12–17]. For example, HREE-related granites are mainly muscovite/biotite monzogranites and two-mica granites [15–17], which are typically accompanied by alterations, including albite, greisen, topaz, fluorite, and sericite [10,19]. Regarding geochemical characteristics, these granites are silica-rich (SiO_2: 72%–78%), peraluminous (A/CNK $\geq$ 1.1), and relatively low in phosphorus (<0.08% P_2O_5). Additionally, they are always predominantly composed of HREEs [10,18,20,21]. The weathering process is also vital for the formation of IAREDs, as it strictly controls REE mineralization in two key aspects. First, the weathering process dramatically facilitates the dissolution of minerals and the liberation of elements. On the other hand, the scavengers of REEs (e.g., clays, carbonates, and Fe–Mn oxides) formed during the weathering process can largely preserve REEs in the regolith through ion exchange, electrostatic interaction, surface complexation, structural incorporation, and secondary precipitation [4,13,14,22–24]. However, the fractionation and fixation of REEs usually occur simultaneously, owing to their different geochemical behaviors during weathering, which is the main controlling factor for REE patterns in the regolith [4,25,26].

The characteristics of bedrock and the weathering process are prerequisites for the generation of IAREDs. However, the mechanisms restricting the formation of HREE deposits have not yet been well studied. To better understand the metallogenic mechanisms of HREE deposits, an integrated and representative profile of an ion-adsorption HREE deposit was collected from the Dabu mining area in Jiangxi Province, South China. Because HREE-rich granites are widely distributed in the studied area and the minerogenetic conditions in the region are favorable, this study conducted microscopic observations, along with mineralogical and geochemical analyses, to investigate material variations in the profile during the weathering process. Furthermore, the characteristics of the bedrock

and the REE fractionation mechanisms were discussed. The results will provide a theoretical basis for understanding the formation mechanisms of such deposits.

2. Geological Background

The Dabu HREE deposit is located on the southeast margin of the Ganzhou Basin in the Nanling area of South China [20]. Its tectonic position is in the southeast of the tectonic magmatic belt of the Eurasian Plate, close to the Pacific Plate. Tectonic magmatic activity is frequent in this area, and ore-forming rock masses rich in REEs are widely distributed, especially Yanshanian granite (Figure 2). The main REE ore-forming parent rock in the region is the Dabu granitic pluton, which occurs in a batholith with an outcrop area of 515 km^2 [20,27]. The Dabu batholith is a multistage complex pluton that was first formed during the Caledonian stage, with a zircon U–Pb age of 393 ± 27 Ma [28]. However, the main part of the Dabu pluton was formed in the early Yanshanian period (161–169 Ma) [29,30].

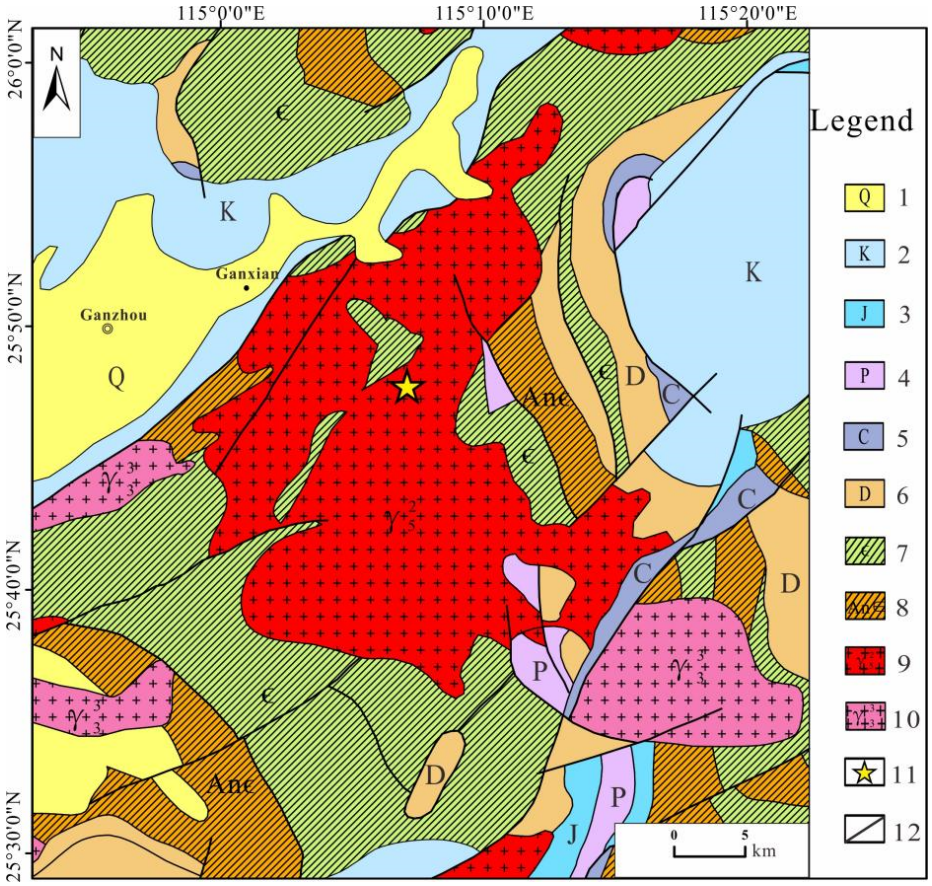

Figure 2. Simplified Geological map showing the distribution of the Dabu granite, with the location of the Dabu profile (modified by 1:2,500,000 geological map of China). 1—Quaternary sediments; 2—Cretaceous conglomerate and sandstone; 3—Jurassic sandstone and mudstone; 4—Permian sandstone; 5—Carboniferous limestone; 6—Devonian sandstone; 7—Cambrian metasandstone; 8—Precambrian metamorphic rocks; 9—Early Yanshanian granite; 10—Late Caledonian granite; 11—the Dabu deposit; 12—Faults.

The Dabu batholith is composed of medium- to coarse-grained biotite granites and medium- to fine-grained muscovite granites. Biotite granites are the main component of the batholith and were formed during the Silurian and the early and late Jurassic periods [30]. The biotite granites from different periods have similar petrographic characteristics, exhibiting flesh-red, off-white color and typical granite structure [31]. The mineral composition includes feldspar (30%–50%), quartz (30%–60%), biotite (5%–10%), and minor muscovite

(0%–1%). The main REE-bearing accessory minerals are zircon, apatite, monazite, thorite, and xenotime [29].

3. Sampling and Analytical Methods

3.1. Description of Regolith Profile and Sampling

The studied samples were taken from a weathering profile on the hilltop, with a depth of 27 m (Figure 3). According to the degree of weathering, mineral compositions, and structure, the weathering profile is divided into the following:

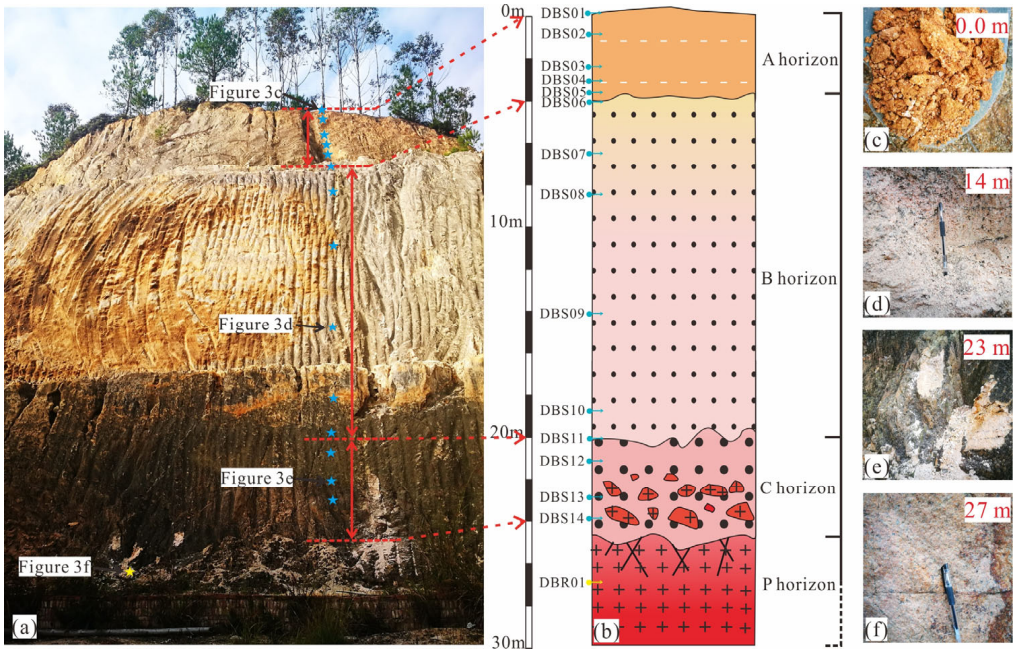

Figure 3. (**a**) Schematic of the weathering profile and (**b**) sampling sites of the Dabu deposit; (**c**–**f**) are the photographs of A, B, C, and P horizon, respectively.

A horizon: This layer is yellowish-brown with strong cohesiveness and is mainly composed of clays and quartz. Samples DBS01–DBS06 were collected from this horizon at depths of 0–4 m. B horizon: This layer commonly appears light flesh-red with a loose structure, and the content of residual feldspar is noticeably increased. Samples DBS07–DBS11 were collected from this horizon at depths of 4–20 m. C horizon: This layer gradually transitions from the B horizon without a distinct boundary. It typically maintains a dense granite structure. Samples DBS12–DBS14 were taken from this horizon at depths of 20–24 m. P horizon: Fresh granite sample DBR01 was collected from this profile at a depth of 27 m. Additionally, fresh granite samples DBR02 and DBR03, as well as weakly weathered granite sample DBR04, were collected near the studied profile. In total, 14 regolith samples and 4 parent rock samples were collected.

3.2. Analytical Methods

The mineral composition of the regolith was analyzed using an X'Pert Pro DY2198 X-ray diffractometer at the China University of Geosciences, Wuhan. The analysis was conducted with Cu Kα radiation at an accelerating voltage of 40 kV and a beam current of 40 mA. The scan range (2θ) was from 3° to 65° at a scan speed of $8°\cdot min^{-1}$. The X-ray diffraction (XRD) patterns were analyzed using JADE 6.0 software to obtain quantitative mineral composition data.

Mineralogical microscope and scanning electron microscope observations of the samples were conducted using a Zeiss Axio Scope A1 and a Zeiss Sigma 500, respectively, at the Key Laboratory of Geochemical Exploration in Langfang, China. Prior to analysis, the samples underwent slicing, polishing, and carbon coating. The instruments operated at a

vacuum of 2×10^{-6} for the working system and 6×10^{-9} mbar for the gun vacuum, with a high voltage of 10 kV and an approximate working distance of 8.5 mm. Both secondary electron and backscatter detectors were used for observations.

The measurements of REE speciation, major elements, and trace elements were conducted at the central laboratory of the Institute of Geophysical and Geochemical Exploration in Langfang, China. The major elements in soil and rock samples were analyzed using a PW4400/40 X-ray fluorescence spectrometer [32,33]. The empirical coefficient method and scattering line internal standard method were employed to correct the matrix effects between the elements [33]. The analytical precision for all major elements was better than 5%. The concentrations of trace elements, including all REEs, were measured using a Thermo Icap Qc inductively coupled plasma mass spectrometer, following the detailed procedures described by [34]. A seven-step sequential extraction routine was conducted to quantify the different speciations of REEs in the Dabu weathering profile [35,36]. The REEs in various occurrence states were continuously extracted into the solution using different reagents, and inductively coupled plasma mass spectrometry was employed to determine the REE content in the solution after each step. Briefly, the reacted REEs at each step were assumed to correspond to the following fractions: the water-soluble fraction (F1), extracted by purified H_2O in step 1; the ion-exchangeable fraction (F2), extracted by $MgCl_2$ solution in step 2; the carbonate-binding fraction (F3), extracted by NaAc solution in step 3; the humic acid fraction (F4), extracted by $Na_4P_2O_7$ solution in step 4; the Fe–Mn oxide fraction (F5), extracted by $NH_2OH{\cdot}HCl$-HCl solution in step 5; the organic matter fraction (F6), extracted by H_2O_2 solution in step 6; and the residual fraction (F7), extracted by a solution of HCl, HNO_3, and H_2O in step 7 [14].

3.3. Mass Transfer Calculations

The mass transfer coefficient is commonly used to accurately evaluate the enrichment or loss of elements from weathered materials in relation to the parent material [37,38].

The formula is as follows:

$$\tau_{j,w} = (C_{j,w}/C_{i,w})/C_{j,p}/C_{i,p}) - 1 \quad (1)$$

where $C_{j,w}$ and $C_{j,p}$ represent the concentrations of the mobile element (j) in the weathered material and parent material, respectively, and $C_{i,w}$ and $C_{i,p}$ represent the concentrations of the immobile element (i) in the weathered material and parent material, respectively. If $\tau_{j,w} > 0$, it indicates that element (j) is enriched in the weathering crust relative to the bedrock; if $\tau_{j,w} < 0$, it indicates that element (j) is leached from the weathering crust relative to the bedrock. Titanium was selected as the inert element, owing to its extremely low solubility in aqueous solutions, relatively high concentration, and uniform distribution in granite [38].

4. Results

4.1. Characteristics of Bedrock

4.1.1. Petrology

The bedrock consists of fine- to medium-grained biotite monzogranite with a massive structure, generally exhibiting a flesh-red color. The fresh granite is composed of K-feldspar (35%), plagioclase (30%), quartz (25%), biotite (9%), and minor muscovite (1%), as illustrated in Figure 4a. Secondary minerals include sericite, clays, muscovite, and precipitated iron.

K-feldspar exhibits semi-euhedral columnar crystals with medium grain size (2–5 mm) and is typically metasomatized by muscovite and clays (Figure 4a,b). Plagioclase appears as semi-euhedral plates with medium grain size (2–4.5 mm) and is usually metasomatized by muscovite, sericite, and minor clays (Figure 4b). Quartz commonly occurs as irregular granules (2–5 mm) distributed around feldspar. Biotite and muscovite present as flaky aggregates (0.25–2 mm) that are sporadically distributed among other minerals; moreover, biotite is often metasomatized by chlorite and sericite

Alterations of feldspars are common in Dabu granites, with some being completely replaced by muscovite aggregates (Figure 4a). This indicates that hydrothermal alterations are intense during the diagenetic process of Dabu granites.

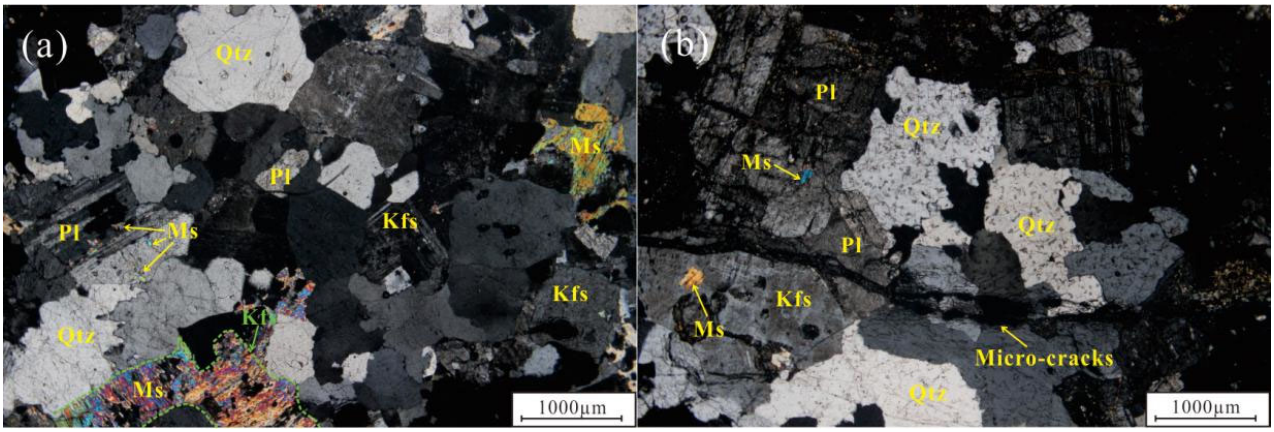

Figure 4. Micro-photographs of the parent granites. (**a**) mineral components of fresh granite; (**b**) weakly weathered granite (etch pits on minerals surfaces and micro-cracks are common). (Abbreviations: Qtz—Quartz, Ms—Muscovite, Kfs—K feldspar, Pl—Plagioclase).

4.1.2. Petrogeochemistry

To better understand the characteristics of ore-forming parent rocks in South China, geochemical data from typical REE-related granites were collected. The element contents of the Dabu granites are listed in Table 1. The results indicate that the Dabu granites have relatively high SiO_2 (74.5%–76.4%) and K_2O + Na_2O (7.3%–8.2%). However, the contents of Al_2O_3, TFe_2O_3, MgO, CaO, and $Mg^{\#}$ are relatively low, measuring 11.9%–12.3%, 0.51%–1.23%, 0.03%–0.13%, 0.18%–0.64%, and 7–18, respectively. In the A/NK-A/CNK diagram (Figure 5a), the LREE-related granites are mainly metaluminous, while the Dabu granites and other HREE-related granites are peraluminous. Additionally, the former are predominantly shoshonitic, whereas the latter are high-K and calc-alkaline (Figure 5b). As a result, the granites that generate HREE deposits are characteristic of a typical peraluminous, high-K, calc-alkaline granite series.

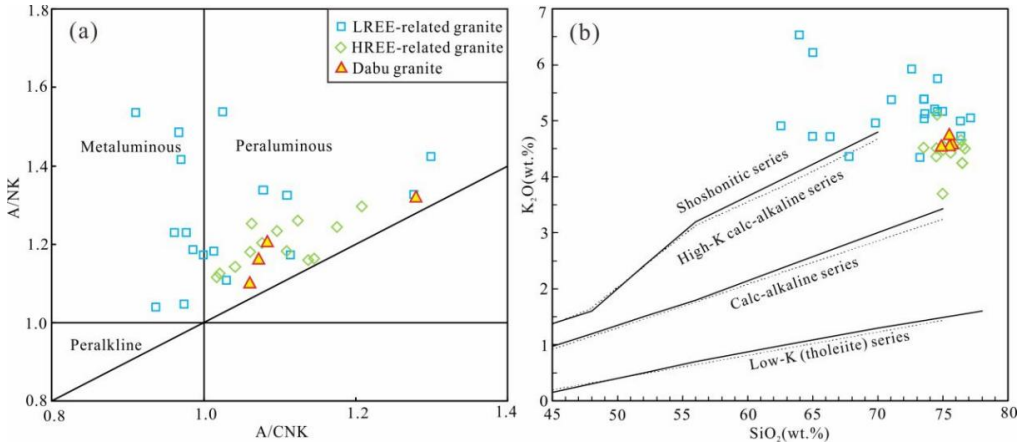

Figure 5. (**a**) A/NK vs. A/CNK and (**b**) SiO_2 vs. K_2O for the Dabu granites and other typical REE-ore-related granites from South China (data were collected from [10,13,15,18,20,21,27,32,39–51]).

Table 1. Major element composition of regolith and bedrock samples (%).

Sample	SiO_2	Al_2O_3	TFe_2O_3	MgO	CaO	Na_2O	K_2O	MnO	P_2O_5	TiO_2	CIA
DBS01	52.3	28.8	3.40	0.15	0.06	0.03	0.77	0.03	0.02	0.31	96.8
DBS02	55.6	27.7	2.24	0.12	0.06	0.03	0.75	0.05	0.02	0.14	96.8
DBS03	48.9	31.4	3.28	0.15	0.06	0.04	0.75	0.03	0.02	0.23	97.1
DBS04	60.8	25.6	2.00	0.12	0.07	0.03	0.71	0.03	0.02	0.13	96.7
DBS05	54.6	28.0	2.59	0.14	0.06	0.03	0.65	0.07	0.02	0.18	97.2
DBS06	56.2	29.3	0.86	0.06	0.06	0.07	2.00	0.14	0.01	0.09	92.4
DBS07	56.2	29.7	0.72	0.06	0.06	0.08	2.43	0.34	0.01	0.06	91.2
DBS08	66.1	20.9	0.80	0.08	0.06	0.10	4.96	0.15	0.01	0.05	78.7
DBS09	60.8	24.3	0.76	0.05	0.06	0.14	5.82	0.12	0.01	0.06	78.5
DBS10	64.7	22.8	0.50	0.05	0.06	0.17	5.83	0.10	0.01	0.05	77.3
DBS11	62.1	24.0	0.81	0.04	0.07	0.20	5.93	0.21	0.01	0.05	77.8
DBS12	67.3	20.5	0.59	0.03	0.06	0.18	5.72	0.13	0.01	0.05	75.7
DBS13	70.8	18.4	0.64	0.04	0.10	0.69	5.26	0.11	0.01	0.04	72.3
DBS14	72.6	15.6	0.57	0.04	0.11	1.55	5.23	0.09	0.01	0.04	72.6
DBR01	76.4	11.9	0.51	0.03	0.24	3.54	4.63	0.07	0.01	0.03	51.4
DBR02	74.5	12.0	1.23	0.13	0.64	3.08	4.51	0.07	0.03	0.09	52.0
DBR03	75.8	12.1	0.75	0.04	0.48	3.31	4.57	0.11	0.01	0.03	51.7
DBR04	76.1	12.3	1.47	0.05	0.18	2.49	4.77	0.08	0.01	0.03	56.1

The total REE content of fresh parent rocks ranges from 178 ppm to 222 ppm (average = 204 ppm), which is slightly lower than the average value (229 ppm) for granites in South China [52]. This suggests that secondary enrichment during weathering is also crucial for REE mineralization. The Dabu granites exhibit significant HREE enrichments (LREE/HREE = 0.2–0.66), along with strong Eu negative anomalies (δEu = 0.04–0.2) and negligible Ce anomalies (δCe = 0.96). The chondrite-normalized REE patterns of the Dabu granites are consistent with those of other HREE-related granites, characterized by a slightly left-inclined pattern and stronger negative Eu anomalies compared with LREE-related granites (Figure 6a). The primitive mantle-normalized trace element diagrams indicate that the HREE-rich granites are enriched in Rb, Th, and U, while being depleted in Ba, Sr, P, and Ti (Figure 6b).

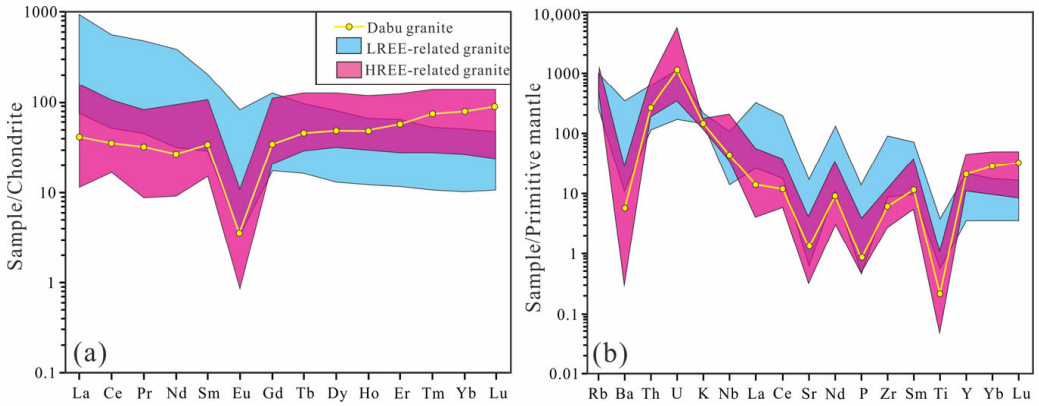

Figure 6. (**a**) Chondrite-normalized REE patterns and (**b**) primitive mantle-normalized trace element diagrams for the Dabu granites and other typical REE-ore-related granites (data were collected from [10,13,15,18,20,21,27,32,39–51]). Chondrite and primitive mantle values are from [53].

4.2. Material Variations of Dabu Granite in Weathering Profile

4.2.1. Mineral Compositions

The chemical index of alteration (CIA = [Al_2O_3/(Al_2O_3 + CaO + K_2O + Na_2O)] × 100%) [54] is used to quantify the weathering degree in the studied profiles. The CIA values for the A, B, and C horizons are 92.4–97.2, 77.8–91.2, and 72.6–75.7, respectively (Table 2). From the bottom up, the CIA value gradually increases from 72.6 to 96.1, suggesting that the parent rock has undergone intense weathering. This condition facilitates the decomposition and transformation of minerals, which is essential for REE enrichment in the regolith.

Table 2. Geochemical parameters of REE and pH value of the weathering profile.

Sample	ΣREE (ppm)	ΣLREE (ppm)	ΣHREE (ppm)	ΣLREE/ΣHREE	δEu	δCe	pH
DBS01	191	67	124	0.55	0.18	1.17	4.44
DBS02	232	111	121	0.92	0.17	2.97	4.64
DBS03	197	96	101	0.95	0.17	2.55	4.73
DBS04	192	72	120	0.60	0.15	2.10	4.60
DBS05	235	123	112	1.10	0.17	3.79	4.60
DBS06	156	71	85	0.83	0.15	2.57	4.87
DBS07	460	186	274	0.68	0.11	0.86	4.91
DBS08	799	266	533	0.50	0.09	0.40	4.65
DBS09	797	164	633	0.26	0.07	0.37	5.47
DBS10	706	117	589	0.20	0.06	0.19	5.32
DBS11	517	103	414	0.25	0.06	0.53	5.59
DBS12	449	78	372	0.21	0.05	0.52	5.41
DBS13	386	69	318	0.22	0.05	0.77	4.96
DBS14	396	66	330	0.20	0.04	0.49	5.57
DBR01	178	37	141	0.26	0.04	0.96	
DBR02	210	84	127	0.66	0.2	0.96	
DBR03	222	38	184	0.20	0.06	0.96	
DBR04	500	69	430	0.16	0.04	0.28	

Plagioclase is susceptible to weathering and, as a result, it completely disappears in the C horizon (Figure 7). K-feldspar, carbonates, and illite completely decompose with the increasing degree of weathering, particularly at the top of the B horizon. Ultimately, only quartz (85%) and clay minerals (15%) remain under extremely intense weathering conditions. The composition of the clay minerals can be determined from the XRD results of the formamide-treated samples. The proportion of halloysite gradually decreases from the bottom (81%) to the upper A horizon (4%), which aligns with the microscopic observations (Figure 8a–d). Halloysite aggregates grow alongside kaolinite below the A horizon; however, halloysite completely disappears in the A horizon. Since halloysite is relatively unstable, it transforms into thermodynamically stable kaolinite through the unrolling of its edges as weathering continues [4,10]. In the early stages of weathering, aluminosilicate minerals continuously decompose and transform into 2:1 type clays (such as illite). As weathering progresses, the unstable 2:1 type clays gradually transform into 1:1 type clays (such as halloysite and kaolinite). Consequently, illite tends to disappear during the weathering process, comprising only 1% in the upper A horizon, as illustrated in Figure 7.

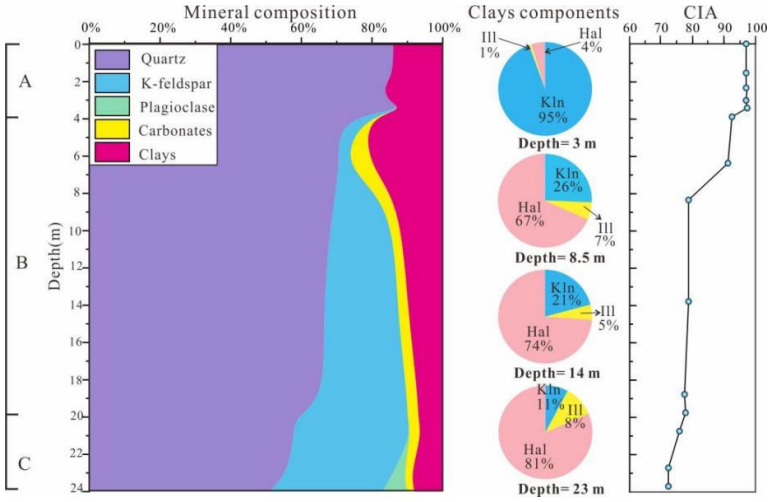

Figure 7. The variations of minerals and CIA value in the Dabu regolith. (Abbreviations: Kln—kaolinite, Hal—halloysite, Ill—illite).

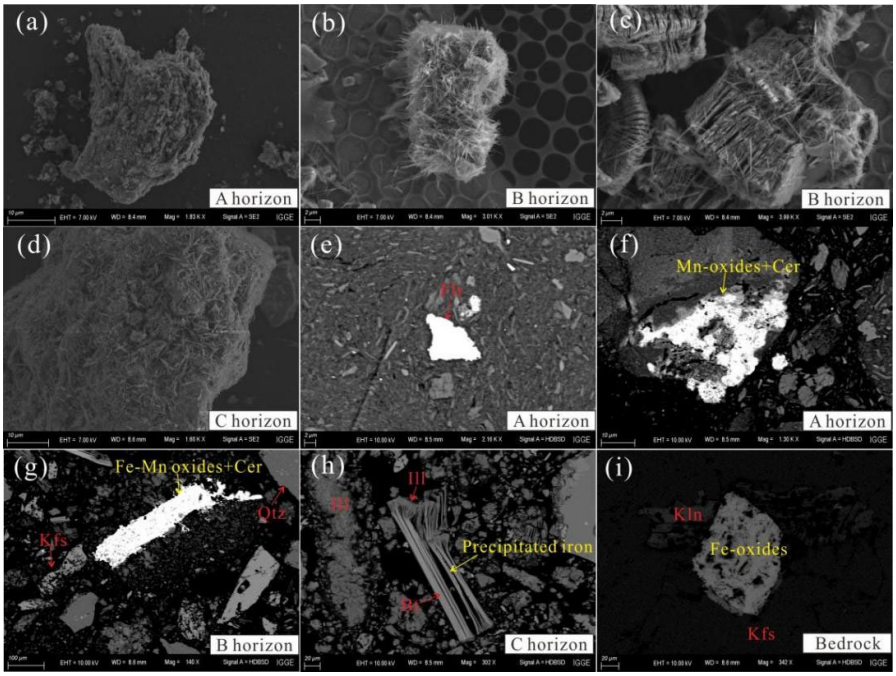

Figure 8. (**a**–**d**) Micro-photographs of clays. (**a**) vermicular kaolinite in A horizon; (**b**) tube-shaped halloysite aggregates in B horizon; (**c**) halloysite aggregates grow at the edge of kaolinite in B horizon; (**d**) Illite aggregates in C horizon; (**e**) secondary florencite in topsoil. (**f**–**i**) micro-photographs of Fe–Mn oxides. (**f**) Mn oxides co-exist with cerianite; (**g**) the aggregations of Fe–Mn oxides and cerianite; (**h**) biotite released iron and transformed into illite; (**i**) the occurrences of kaolinite and Fe-oxides in bedrock. (Abbreviations: Bt—biotite, Cer—cerianite, Flr—florencite, Ill—illite, Kln—kaolinite, Kfs-K—feldspar, Qtz—quartz).

4.2.2. Major Elements

As illustrated in Figure 9 and Table 1, Na_2O and CaO are almost entirely removed from the regolith in the C horizon, owing to the rapid decomposition of plagioclase. The concentration coefficients for these elements decreased to their minimum values at the surface (−1 and −0.98, respectively). The weathering resistance of biotite and K-feldspar is slightly stronger than that of plagioclase, resulting in the concentration coefficients of MgO and K_2O gently decreasing to their minimum values (−0.51 and −0.99, respectively)

at the surface. The variations in MnO and P_2O_5 are similar to those of MgO and K_2O, with minimum values of −0.97 and −0.87, respectively. Quartz is extremely stable during weathering; therefore, the removal of SiO_2 is mainly related to the depletion of silicate minerals. The minimum concentration coefficient for SiO_2 is −0.94, indicating that a significant amount of silicate minerals decomposed to form clays. The removals of Al_2O_3 and TFe_2O_3 are relatively inconspicuous below the A horizon; however, depletion becomes more pronounced at the surface, with minimum values of −0.79 and −0.41, respectively.

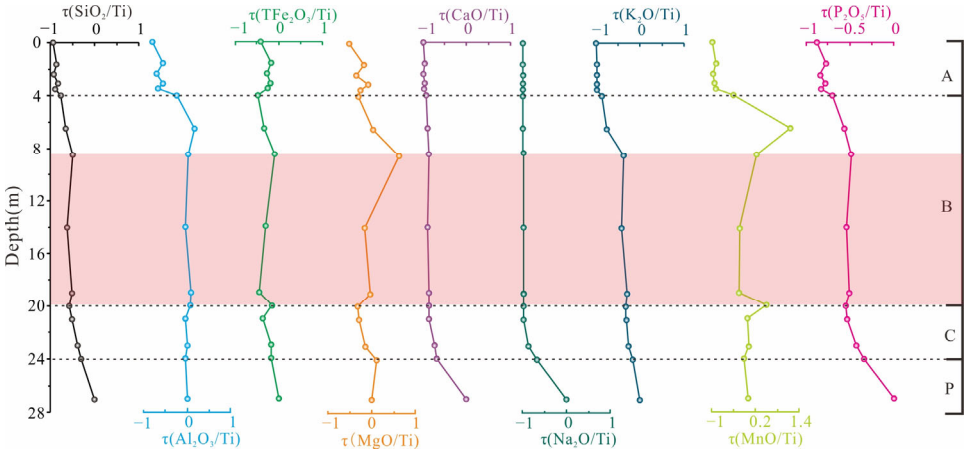

Figure 9. Mass transfer coefficient ($\tau_{Ti,j}$) of major element in the Dabu profile. (The red shaded area represents the REE-rich horizon, at a depth of 8.5–20.0 m).

4.2.3. Distribution of REEs

The REE patterns of the regolith are mainly inherited from the parent rocks, displaying a left-inclined pattern with a clear negative Eu anomaly (Figure 10). However, there are notable variations among the different horizons. Compared with the B and C horizons, the REE pattern of the A horizon is relatively flat. Additionally, it exhibits a significant positive Ce anomaly, in contrast to the negative Ce anomalies observed in the B and C horizons. This suggests that the surface horizon is relatively rich in LREEs, particularly Ce.

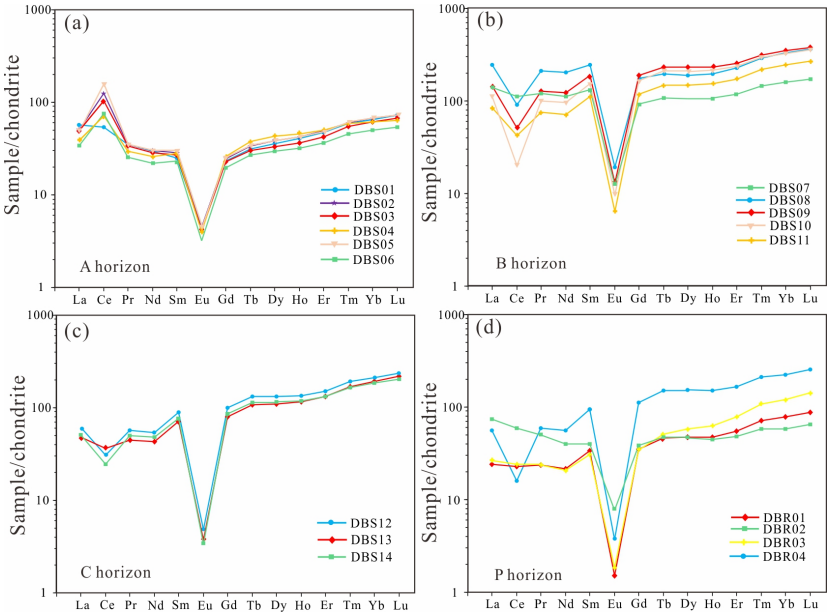

Figure 10. Chondrite-normalized REEs pattern for regolith (**a**–**c**) and bedrock samples (**d**). Chondrite values are from [53].

No significant variations exist in the total REE content (ΣREE) in the A horizon, which remains below 250 ppm (ranging from 156 to 235 ppm). However, ΣREE rapidly increases to a maximum of 799 ppm in the upper B horizon (at a depth of 8.5 m), followed by a gradual decrease to 396 ppm at the bottom of the C horizon (at a depth of 24 m). Ultimately, an 11.5 m ore body forms at depths ranging from 8.5 m to 20 m. Notably, the pH value continuously increases from 4.4 at the surface to 5.6 at the bottom of the regolith, with a particularly significant growth trend observed in the REE-rich horizon. As illustrated in Figure 11, the variation trends of ΣHREE and ΣLREE are similar to that of ΣREE, displaying a significant increase followed by a gradual decline from the top down. However, ΣLREE reaches its maximum (266 ppm) at a depth of 8.5 m, while ΣHREE peaks (633 ppm) at a depth of 14 m.

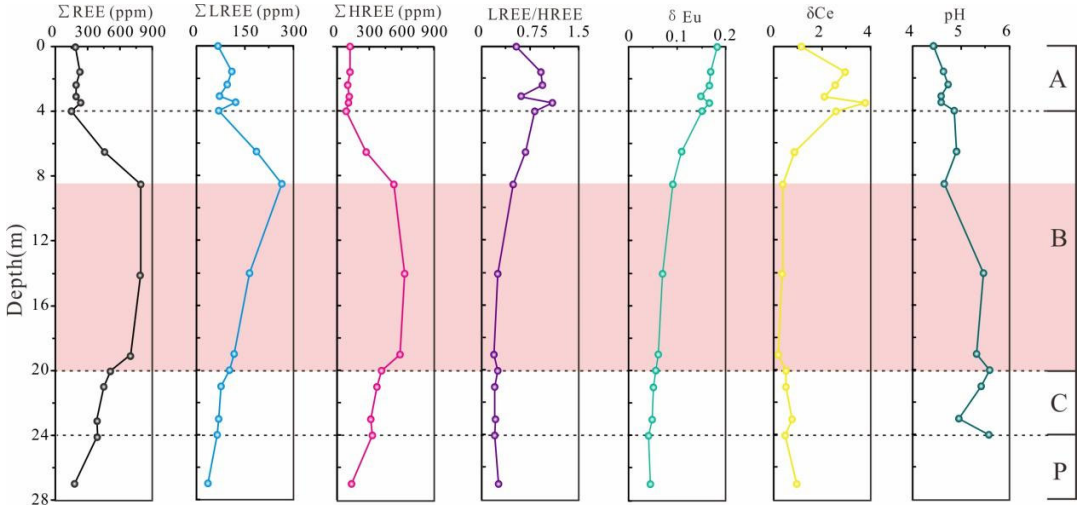

Figure 11. Vertical variations of REEs indices (ΣREE, ΣLREE, ΣHREE, ΣLREE/ΣHREE, δEu, and δCe) and pH values in the Dabu weathering profile. The red shadow represents the REE-rich horizon.

The A horizon exhibits a positive Ce anomaly (δCe = 1.17–3.79); however, this transforms into a negative anomaly (δCe = 0.19–0.86) in the lower horizons. Owing to the significant accumulation of Ce at the surface, the LREE/HREE ratio is relatively high within the A horizon (0.55–1.1), followed by a gradual decrease in the deeper horizons (0.83–0.2). The δEu value continuously declines from 0.18 at the top to 0.04 at the bottom.

4.2.4. Speciation of REEs

The geochemical properties of REEs during weathering are similar, resulting in consistent trends for LREE and HREE speciation throughout the entire regolith. The total REE in the regolith mainly exists in the ion-exchangeable fraction (23.7%–69.2%) (Figure 12), followed by the residual fraction (13.8%–67.7%), carbonate-binding fraction (F3) (3.05%–23.9%), and the Fe–Mn oxide fractions (1.97%–21.1%). However, the humic acid (<2%), organic matter (<5%), and water-soluble fractions (<0.05%) constitute only a minor portion of the total REE concentrations.

From the surface down, the proportions of exchangeable LREEs and HREEs increased to their maximum (67.9% and 69.7%, respectively) before gradually declining. Notably, these proportions are highest in the REE-rich horizon (46.6%–67.9% for LREEs and 58.8%–69.7% for HREEs) compared with the entire regolith. As one moves downward, the proportion of the residual total REE gradually decreases from 67.7% to 23.1%. Interestingly, a significantly larger amount of HREEs occurs in the residual fraction compared with LREEs throughout the entire regolith. The residual fraction accounts for 14.3% to 43.8%, with an average of 21.1% in LREE speciation, compared with 17.1% to 79.8%, with an average of 43.6% in HREE speciation. The proportion of Fe–Mn oxide in LREEs (4.17% to 37%, with an average of 21.5%) is significantly higher than that of HREEs (0.95% to 3.99%,

with an average of 2.5%) in the Dabu regolith. The proportions of carbonate-binding LREEs and HREEs consistently decreased from the bottom (20% and 24.5%, respectively) to the surface (5.79% and 2.33%, respectively).

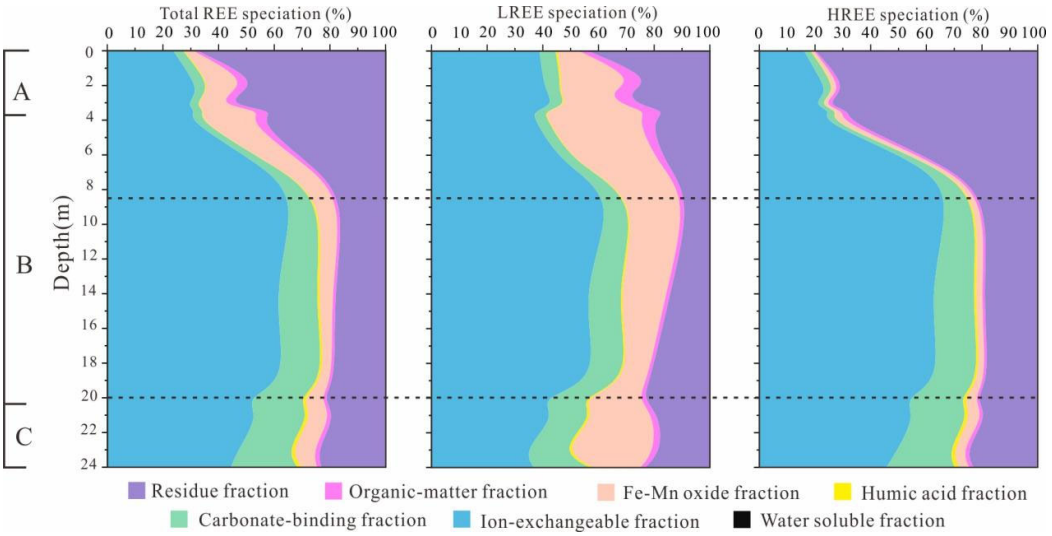

Figure 12. Variations in total REE, LREE and HREE speciations with depth in the Dabu weathering profile. (The black dotted lines represent REE-rich horizon).

5. Discussion

5.1. REEs Fractionation

The fractionation of REEs is a common phenomenon during both endogenic processes and the chemical weathering of bedrock, owing to their different geochemical behaviors [3,4,25,26,38]. The fractionation process mainly occurs through the following five geochemical mechanisms:

1. Fractional crystallization of magma and hydrothermal alterations of bedrock: The depletion of P, Ti, Ba, and Sr (Figure 6b) may indicate the fractional crystallization of apatite, Ti-bearing minerals, and plagioclase, respectively [25]. As fractional crystallization occurs, the residual melt becomes enriched in HREEs and depleted in Eu. Additionally, hydrothermal alterations play a crucial role in HREE concentration in granite and the subsequent ore genesis during weathering [6,12,55]. On the one hand, REEs introduced by hydrothermal processes can increase the total REE content [6] and even alter the REE patterns of parent rocks. For example, the transformation of biotite K-feldspar granite to muscovite potassium-alkali feldspar granite results in an increase in HREE/LREE from 1.2:1 to 4:1 in the Zudong granites [19,41]. On the other hand, hydrothermal processes can leach REEs from weathering-resistant REE-bearing minerals (e.g., monazite and xenotime), which are subsequently scavenged by weathering-prone REE minerals (apatite, allanite, and REE-fluorocarbonates) [10,19,41].

2. Differential weathering of REE-bearing minerals: Previous studies indicate that the weathering resistance of REE-bearing minerals follows this sequence—fluorocarbonate < silicate < niobotantalate < arsenate < phosphate [55]. The REE patterns of these minerals also vary significantly. Among the common REE-bearing accessory minerals, thorite, xenotime, zircon, and fergusonite are rich in HREEs, while monazite, apatite, parisite, titanite, and allanite are rich in LREEs [10,14,15,41,56]. Therefore, their differential dissolution will inevitably lead to the fractionation of REEs [25]. The average proportion of the residue fraction for HREEs (43.6%) is significantly higher than that of LREEs (21.1%) in the Dabu regolith (Figure 12), suggesting that HREE-enriched minerals are much more stable during weathering. This stability contributes to the pronounced REE fractionation observed in the regolith.

3. Migration of REEs in regolith: REEs mainly migrate as ligand complexes with fluids in the regolith [40]. Groundwater contains various anions, such as HCO_3^-, CO_3^{2-}, SO_4^{2-}, NO^{3-}, F^-, and Cl^-, which provide abundant inorganic ligands for the migration of REEs [22,57]. Additionally, REEs can combine with organic matter to form organic complexes [58,59]. Both inorganic and organic ligand complexes of HREEs are more stable than those of LREEs, owing to their smaller ionic radii [60,61]. As a result, HREEs tend to accumulate in the deeper horizons (Figure 11). This phenomenon accounts for the decrease in ΣLREE/ΣHREE from the upper B horizon (0.83) to the bottom of the regolith (0.2).

4. Selective adsorption and complexation of scavengers: Kaolinite and halloysite are the primary adsorption carriers for REEs, as shown in Figures 7, 11 and 12. Together, they account for more than 90% of the clay component in the REE-rich horizon. Previous studies have indicated that at low ionic strengths (I = 0.01 M $NaHNO_3$), clays mainly adsorb REEs through ion exchange, with no significant REE fractionation occurring [23,62–64]. However, at high ionic strengths (I = 0.5 M $NaHNO_3$), HREEs are preferentially complexed by clays. The adsorption and complexation of Fe–Mn oxides and CO_3^{2-} with REEs are typically selective, owing to the different ionic radii of the REEs [3,62,65–69]. REEs are mainly fixed by Fe–Mn oxides through inner-sphere complexation [3]. With their smaller ionic radii and stronger hydrolysis abilities, HREEs are preferentially complexed by Fe–Mn oxides and CO_3^{2-} [68,69].

5. Precipitation of secondary REE-bearing minerals: As a variable valence element, Ce is more susceptible to redox conditions compared with other REEs [22]. Ce^{3+} can be oxidized to Ce^{4+}, which then hydrolyzes to form insoluble cerite (CeO_2) in oxidizing conditions, leading to its separation from other REEs in the superficial horizon [10,22,70]. Additionally, Ce^{3+} can be oxidized by Fe–Mn oxides to form aggregations [71–73], as shown in Figure 8f,g. The regolith contains more abundant (Bi) carbonate complexes compared with other inorganic complexes such as SO_4^{2-}, Cl^-, and F^- [60,74]. The product of the concentrations of REE^{3+}, CO_3^{2-}, and F^- in fluids can easily exceed the K_{sp} value of REE-fluorocarbonate, resulting in the precipitation of these minerals. However, REE-fluorocarbonate is susceptible to weathering [26], which explains the continuous decrease in the proportion of carbonate-bonded REE from the bottom (23.9%) to the surface (3.49%) (Figure 12). In contrast, secondary florencite is resistant to weathering and is preserved in the A horizon (Figure 8e). Consequently, the formation of secondary REE-bearing minerals is significant for REE fractionation.

5.2. Ore-Forming Process

1. Initial stage: At the onset of weathering, rock-forming minerals that are susceptible to weathering, such as plagioclase and biotite, dissolve and transform into 2:1 type clay, mainly illite (Figure 8h). These clays have a large specific surface area (SSA) and provide abundant adsorption sites for REEs [66]. During this stage, a certain amount of Fe oxides is precipitated from the primary Fe oxide minerals (e.g., magnetite and ilmenite) and Fe-bearing silicate minerals (e.g., biotite). Mn, usually present as a trace element, leaches with Fe oxides and forms Fe–Mn (hydr)oxides through oxidation and precipitation (Figure 8h,i) [3]. Fe–Mn oxides are crucial for the enrichment of HREEs, owing to their preferential adsorption of HREEs [68,69]. Crystalline Fe oxides exhibit stronger selective adsorption of HREEs compared with amorphous Fe oxides; however, the latter has a higher adsorption capacity because of its larger SSA [75,76]. Both illite and Fe–Mn oxides are excellent scavengers of REEs, owing to their relatively high adsorption capacities, as previously mentioned. Therefore, they are indispensable for the fixation of iREEs in the early stages of weathering (Figure 13a).
2. Intermediate stage: As weathering progresses, many minerals in parent rocks continuously decompose, leading to the release of elements from minerals. Mobile major elements (e.g., Na^+, Ca^{2+}, K^+) are largely removed by weathering fluids from the regolith (Figure 13b). Conversely, REEs are mainly fixed by clays and Fe–Mn ox-

ides through ion exchange, electrostatic interaction, surface complexation, structural incorporation, or formation of secondary minerals (such as florencite and cerianite) in the regolith [13,14,22–24,77]. These processes often cause significant REE fractionation, owing to the different geochemical behaviors of REEs during weathering [2–4,10,22–24,38,65]. Intensified weathering also accelerates the transformation from 2:1 type clays (mainly illite) to 1:1 type clays (e.g., kaolinite and halloysite). Illite has a larger SSA and stronger cation exchange capacity than kaolinite and halloysite [66,77]. However, the relative content of illite is much lower than that of kaolinite and halloysite in REE-rich horizons (Figures 7, 11 and 12). Therefore, REEs are mainly adsorbed by kaolinite and halloysite.

3. Advanced stage: Under conditions of intense chemical weathering, rock-forming minerals almost completely decompose, except for quartz (Figure 7). At this stage, major elements are massively removed from the regolith by fluids (Figure 9). The REE-bearing minerals that can be weathered completely dissolve, serving as the main source of iREEs. However, weathering-resistant REE-bearing minerals (e.g., zircon, xenotime, and monazite) retain REEs in the residue fraction. Since halloysite is relatively unstable under intense weathering, it transforms into thermodynamically stable kaolinite by unrolling its edges. This process results in the adsorbed REEs located in the internal and lumen pores being directly exposed to the weathering fluids, making desorption much more feasible [77]. The pH value of the upper regolith is relatively low (4.44–4.65), causing the adsorbed iREEs to be largely exchanged by abundant H^+ [2,42,77–79]. The released iREEs then migrate downward with the fluids. As the pH value increases, the mobility of REE complexes decreases, enhancing the adsorption capacity of clays, organic matter, and Fe–Mn oxides for REEs [57,80–82]. As a result, REEs gradually accumulate in the horizons, where the pH value rapidly increases from 4.65 at a depth of 8.5 m to 5.59 at a depth of 20 m (Figure 11 and Table 2). However, the complexes of HREE are more stable than those of LREEs, causing HREEs to tend to be enriched in the deeper regolith (Figure 13c).

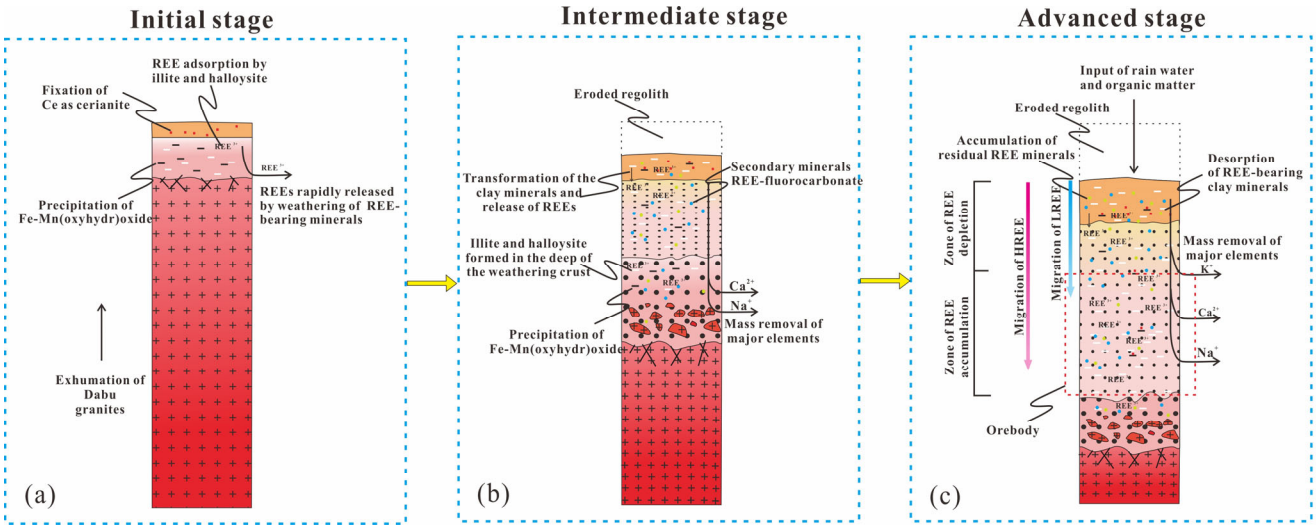

Figure 13. A schematic model illustrating the formation of the Dabu deposit (modified by [10]). (**a**) initial stage: REE were rapidly released from weathering susceptible REE-bearing minerals in weakly weathering condition; (**b**) intermediate stage: with the development of weathering, major elements were greatly removed from regolith and amounts of clays formed; (**c**) advanced stage: REE presented obvious enrichment and fractionation in regolith.

6. Conclusions

The Dabu granites are typical peraluminous, high-K, calc-alkaline granite series with high silica content, relatively low phosphorus content, and high HREE content. The REE

pattern of the regolith is essentially inherited from the parent rocks. The weathering process plays a crucial role in REE mineralization by facilitating the release of REEs and the formation of REE scavengers (e.g., clays, carbonates, and Fe–Mn oxides). The results indicate that the released REEs are mainly adsorbed by kaolinite and halloysite as ion-exchangeable fractions, which account for 49.2%–69.2% of the bulk samples in the REE-rich horizon. The relatively high proportion of the ion-exchangeable fraction makes the Dabu HREE deposit easy to mine and indicates its economic potential. However, the fractionation of REEs often occurs in the regolith, owing to their different geochemical behaviors during the weathering process. In conclusion, the differential weathering of REE-bearing minerals, the mobility of REEs, selective adsorption and complexation of scavengers, and the precipitation of secondary REE-bearing minerals are the main processes responsible for REE fractionation.

Author Contributions: M.X. and J.Z. conceived and designed the ideas; J.Z., B.C. and H.M. collected samples in the field; M.X. wrote the manuscript; J.Z., X.W., Q.H., B.Z., W.W., L.W. and M.T. revised and edited the manuscript; X.D. and H.W. contributed to experimental analysis. All authors have read and agreed to the published version of the manuscript.

Funding: This study was financially supported by the National Nonprofit Institute Research Grant of CAGS (JKYZD202328, JYYWF20182401), and the International Science Cooperation Program of Mapping Chemical Earth (DD20221807).

Data Availability Statement: Data are contained within the article.

Acknowledgments: We are grateful to the reviewers for their valuable comments and recommendations on an earlier version of this paper. We thank the staff of Bureau of Geology and Mineral Exploration and Development of Jiangxi Province for their assistance in the field. We also thank Panlong Wang (Chang'an University) for his constructive suggestions and help.

Conflicts of Interest: The authors declare no conflict of interest.

References

1. Ferhaoui, S.; Kechiched, R.; Bruguier, O.; Sinisi, R.; Kocsis, L.; Mongelli, G.; Bosch, D.; Ameur-Zaimeche, O.; Laouar, R. Rare earth elements plus yttrium (REY) in phosphorites from the Tébessa region (Eastern Algeria): Abundance, geochemical distribution through grain size fractions, and economic significance. *J. Geochem. Explor.* **2022**, *241*, 107058. [CrossRef]
2. Borst, A.M.; Smith, M.P.; Finch, A.A.; Estrade, G.; Villanova-De-Benavent, C.; Nason, P. Adsorption of rare earth elements in regolith-hosted clay deposits. *Nat. Commun.* **2020**, *11*, 4386. [CrossRef] [PubMed]
3. Huang, J.; Tan, W.; Liang, X.; He, H.; Ma, L.; Bao, Z.; Zhu, J. REE fractionation controlled by REE speciation during formation of the Renju regolith-hosted REE deposits in Guangdong Province, South China. *Ore Geol. Rev.* **2021**, *134*, 104172. [CrossRef]
4. Li, Y.H.M.; Zhou, M.F. The role of clay minerals in forming the regolith-hosted heavy rare earth element deposits. *Am. Mineral.* **2020**, *105*, 92–108. [CrossRef]
5. Wang, X.Q.; Zhou, J.; Chi, Q.H.; Wang, W.; Zhang, B.M.; Nie, L.S.; Liu, D.S.; Xu, S.F.; Wu, H.; Gao, Y.F. Geochemical Background and Distribution of Rare Earth Elements in China: Implications for Potential Prospects. *Acta Geosci. Sin.* **2020**, *41*, 747–758.
6. Xu, C.; Kynický, J.; Smith, M.P.; Kopriva, A.; Brtnický, M.; Urubek, T.; Yang, Y.; Zhao, Z.; He, C.; Song, W. Origin of heavy rare earth mineralization in South China. *Nat. Commun.* **2017**, *8*, 14598. [CrossRef]
7. Simandl, G.J. Geology and market-dependent significance of rare earth element resources. *Miner. Depos.* **2014**, *49*, 889–904. [CrossRef]
8. Wang, X.Q.; Zhou, J.; Zhang, B.M.; Liu, D.S.; Xu, S.F.; Wang, W.; Wang, Q.; Qiao, Y.; Xie, M.J.; Liu, F.T.; et al. Finding and Implication of an Undiscovered Giant Deposit of Ion-adsorption Rare Earth Elements in Honghe, South Yunnan, China. *Acta Geosci. Sin.* **2022**, *43*, 509–519.
9. García, M.V.R.; Krzemień, A.; del Campo, M.M.; Álvarez, M.M.; Gent, M.R. Rare earth elements mining investment: It is not all about China. *Resour. Policy* **2017**, *53*, 66–76. [CrossRef]
10. Li, M.Y.H.; Zhou, M.-F.; Williams-Jones, A.E. The genesis of regolith-hosted heavy rare earth element deposits:Insights from the world-class Zudong deposit in Jiangxi Province, South China. *Econ. Geol.* **2019**, *114*, 541–568. [CrossRef]
11. Pan, G.T.; Lu, S.N.; Xiao, Q.H.; Zhang, K.X.; Yin, F.G.; Hao, G.J.; Luo, M.S.; Ren, F.; Yuan, S.H. Division of tectonic stages and evolution in China. *Earth Sci. Front.* **2016**, *23*, 1–23.
12. Chu, G.B.; Chen, H.Y.; Feng, Y.Z.; Wu, C.; Li, S.S.; Zhang, Y.; Lai, C.K. Are South China granites special in forming ion-adsorption REE deposits? *Gondwana Res.* **2024**, *125*, 82–90. [CrossRef]
13. Fu, W.; Li, X.; Feng, Y.; Feng, M.; Peng, Z.; Yu, H.; Lin, H. Chemical weathering of S-type granite and formation of Rare Earth Element (REE)-rich regolith in South China: Critical control of lithology. *Chem. Geol.* **2019**, *520*, 33–51. [CrossRef]

14. Fu, W.; Luo, P.; Hu, Z.; Feng, Y.; Liu, L.; Yang, J.; Feng, M.; Yu, H.; Zhou, Y. Enrichment of ion-exchangeable rare earth elements by felsic volcanic rock weathering in South China: Genetic mechanism and formation preference. *Ore Geol. Rev.* **2019**, *114*, 103120. [CrossRef]
15. Fu, W.; Zhao, Q.; Luo, P.; Li, P.Q.; Lu, J.P.; Zhou, H.; Yi, Z.B.; Xu, C. Mineralization diversity of ion-adsorption type REE deposit in southern China and the critical influence of parent rocks. *Acta Geol. Sin.* **2022**, *96*, 3901–3925.
16. Zhao, Z.; Wang, D.H.; Chen, Z.Y.; Guo, N.X.; Liu, X.X.; He, H.H. Metallogenic speciation of rare earth mineralized igneous rocks in the Eastern Nanling region. *Geotecton. Met.* **2014**, *38*, 255–263.
17. Zhao, Z.; Wang, D.H.; Chen, D.H.; Chen, Z.Y. Progress of research on metallogenic regularity of ion-adsorption type REE deposit in the Nanling range. *Acta Geol. Sin.* **2017**, *91*, 2814–2827.
18. Liu, R.; Wang, R.C.; Lu, X.C.; Li, J. Nano-sized rareearth mineralsfrom granite related weathering-type REE deposits in southern Jiangxi. *Acta Petrol. Mineral.* **2016**, *35*, 617–626, (In Chinese with English abstract).
19. Huang, D.H.; Wu, C.Y.; Han, J.Z. REE Geochemistry and Mineralization Characteristics of the Zudong and Guanxi Granites, Jiangxi Province. *Acta Geol. Sin.-Engl.* **1989**, *2*, 139–157.
20. Wu, K.X.; Zhu, P.; Sun, T.; Chen, L.K.; Ouyang, H.; Xiong, F.K. Study on the Ore-controlling Factors and the Mineralization and Enrichment Features of Dabu HREE Deposit, Southern Jiangxi Province. *Chin. Rare Earths* **2017**, *38*, 1–10.
21. Deng, Z.C. Characteristics and genesis of the Datian HREE granite, southern Jiangxi. *J. Guilin Coll. Geol.* **1988**, *8*, 39–48.
22. Ma, Y.J.; Huo, R.K.; Xu, Z.F.; Zhang, H.; Liu, C.Q. REE behavior and influence factors during chemical weathering. *Adv. Earth Sci.* **2004**, *19*, 87–94.
23. Yang, M.; Liang, X.; Ma, L.; Huang, J.; He, H.; Zhu, J. Adsorption of REEs on kaolinite and halloysite: A link to the REE distribution on clays in the weathering crust of granite. *Chem. Geol.* **2019**, *525*, 210–217. [CrossRef]
24. Yang, M.; Liang, X.; Li, Y.; He, H.; Zhu, R.; Arai, Y. Ferrihydrite transformation impacted by adsorption and structural incorporation of rare earth elements. *ACS Earth Space Chem.* **2021**, *5*, 2768–2777. [CrossRef]
25. Sanematsu, K.; Kon, Y.; Imai, A.; Watanabe, K.; Watanabe, Y. Geochemical and mineralogical characteristics of ion-adsorption type REE mineralization in Phuket, Thailand. *Miner. Depos.* **2013**, *48*, 437–451. [CrossRef]
26. Yang, Y.; Li, G.; Huang, C.; Liu, X.; Wang, X.; Li, C.; Wu, B.; Luo, W. Discovery of supergene REE-fluorocarbonate minerals in weathered spheres of Xiajialing regolith-hosted rare earth element deposit in Xiangshan, Jiangxi Province, South China. *Ore Geol. Rev.* **2023**, *162*, 105712. [CrossRef]
27. Zhang, Q.; Chen, B.F.; Zhang, X.W. Geological, geochemical characteristics and significance of Fengshan HREE deposit in Ganxian district, Jiangxi Province. *East China Geol.* **2020**, *41*, 359–367.
28. Liu, X.Y. *1:50000 Dabu Rigional Geological Survey Report*; Geological Survey of Jiangxi Province: Nanchang, China, 2000.
29. Bureau of Geology and Mineral Resources of Jiangxi Province. *Regional Geology of Jiangxi Province*; Geological Publishing House: Beijing, China, 1982; pp. 373–375.
30. Fang, G.C.; Chen, Z.H.; Chen, Y.C.; Zhao, Z.; Hou, K.J.; Zeng, Z.L.; Luo, Z. Two petrogenetic stages of Dabu composite granite pluton in South Jiangxi and their geological implications. *Miner. Depos.* **2017**, *36*, 1415–1424, (In Chinese with English abstract).
31. Wang, H.; He, H.; Yang, W.; Bao, Z.; Liang, X.; Zhu, J.; Ma, L.; Huang, Y. Zircon texture and composition fingerprint HREE enrichment in muscovite granite bedrock of the Dabu ion-adsorption REE deposit, South China. *Chem. Geol.* **2023**, *616*, 121231. [CrossRef]
32. Wang, X.; Liu, X.; Han, Z.; Zhou, J.; Xu, S.; Zhang, Q.; Chen, H.; Bo, W.; Xia, X. Concentration and distribution of mercury in drainage catchment sediment and alluvial soil of China. *J. Geochem. Explor.* **2015**, *154*, 32–48. [CrossRef]
33. Zhang, Q.; Bai, J.F.; Wang, Y. Analytical scheme and quality monitoring system for China Geochemical Baselines. *Earth Sci. Front.* **2012**, *19*, 33–42.
34. Liu, Y.; Liu, H.C. Simultaneous and precise determination of 40 trace elements in rock samples using ICP-MS. *Geochimica* **1996**, *25*, 552–558.
35. Ma, Y.J. Geochemistry of Trace Elements and Strontium Isotopes in Chemical Weathering. Ph.D. Thesis, Institute of Geochemistry, Chinese Academy of Sciences, Guiyang, China, 1999. (In Chinese).
36. Shi, Y.H.; Qiu, L.; Tang, B.Y.; Yang, Z.P.; Gu, X.Q. Determination of total ionic-phase rare earth and component in ion-adsorption rare earth ore by inductively coupled plasma mass spectrometry. *Metall. Anal.* **2014**, *34*, 14–19.
37. Brimhall, G.H.; Dietrich, W.E. Constitutive mass balance relations between chemical composition, volume, density, porosity, and strain in metasomatic hydrochemical systems: Results on weathering and pedogenesis. *Geochim. Cosmochim. Acta* **1987**, *51*, 567–587. [CrossRef]
38. Nesbitt, H.W. Mobility and fractionation of rare earth elements during weathering of agranodiorite. *Nature* **1979**, *279*, 206–210. [CrossRef]
39. Wu, C.Y. The Study of Ion-Adsorbed Type of Rare Earth Deposits in Weathering Crust from South Jiangxi and North Guangdong Provinces. Ph.D. Thesis, Chinese Academy of Geological Sciences, Beijing, China, 1988.
40. Li, Y.H.M.; Zhao, W.W.; Zhou, M.-F. Nature of parent rocks, mineralization styles and ore genesis of regolith-hosted REE deposits in South China: An integrated genetic model. *J. Asian Earth Sci.* **2017**, *148*, 65–95. [CrossRef]
41. Bao, Z.; Zhao, Z. Geochemistry of mineralization with exchangeable REY in the weathering crusts of granitic rocks in South China. *Ore Geol. Rev.* **2008**, *33*, 519–535. [CrossRef]

42. Huang, J.; Tan, W.; Liang, X.L.; He, H.P.; Ma, L.Y.; Bao, Z.W.; Zhu, J.X.; Zhou, Q. Weathering characters of REE-bearing accessory minerals and their effects on REE mineralization in Renju regolith-hosted REE deposits in Guangdong Province. *Geochimica* **2022**, *51*, 684–695.
43. Zhao, Z.; Wang, D.H.; Bagsa, L.; Chen, Z.Y. Geochemical and REE mineralogical characteristics of the Zhaibei Granite in Jiangxi Province, southern China, and a model for the genesis of ion-adsorption REE deposits. *Ore Geol. Rev.* **2022**, *140*, 104579. [CrossRef]
44. Huang, D.H.; Wu, C.Y.; Han, J.Z. Petrology, rare earth geochemistry and diagenetic mechanism of Zudong and Guanxi granites in Jiangxi Province. *Bull. Chin. Acad. Geol. Sci.* **1993**, *Z1*, 69–94.
45. Murakami, H.; Ishihara, S. REE mineralization of weathered crust and clay sediment on granitic rocks in the Sanyo belt, SW Japan and the southern Jiangxi Province, China. *Resour. Geol.* **2008**, *58*, 373–401. [CrossRef]
46. Ishihara, S.; Hua, R.; Hoshino, M.; Murakami, H. REE abundance and REE minerals in granitic rocks in the Nanling range, Jiangxi Province, southern China, and generation of the REE-rich weathered crustd eposits. *Resour. Geol.* **2008**, *58*, 355–372. [CrossRef]
47. Zhang, B.T.; Wu, J.Q.; Ling, H.F.; Chen, P.R. Magma-dynamic evidence for Indo-sinian cycle emplacement of the Zhaibei and Pitou granite batholith of Nanling range in south China and the tectonic implication. *Contrib. Geol. Miner. Resour. Res.* **2011**, *26*, 119–130.
48. Xie, Z.D.; Yang, Y. Isotopic age and geological significance of Anxi pluton in Xinfeng, Jiangxi Province. *Jiangxi Geol.* **2000**, *14*, 172–175.
49. Zhang, B.; Zhu, X.P.; Zhang, B.H.; Gao, R.D.; Zeng, Z.J.; Ma, G.T. Geochemical Characteristics of Tuguanzhai Ion-Adsorption Type REE Deposit in Tengchong, Yunnan. *J. Chin. Soc. Rare Earths* **2019**, *37*, 491–506.
50. Huang, H.Q.; Li, X.H.; Li, W.X.; Liu, Y. Age and origin of the Dadongshan granite from the Nanling range: SHRIMP U-Pb zircon age, geochemistry and Sr-Nd-Hf isotopes. *Geol. J. China Univ.* **2008**, *3*, 317–333, (In Chinese with English abstract).
51. Chen, B.F.; Zou, X.Y.; Peng, L.L.; Qi, F.Y.; Que, X.H.; Zhang, Q.; Zhou, X.H. Geological characteristics and heavy rare earth Ore prospecting potential of Qingxi Pluton rare earth deposit. *Chin. Rare Earths* **2019**, *40*, 20–31.
52. Shi, C.; Yan, M.; Chi, Q. Abundances of chemical elements of the granitoids in different geotectonic units of China and their characteristics. *Front. Earth Sci. China* **2007**, *1*, 309–321. [CrossRef]
53. Sun, S.S.; McDonough, W.F. Chemical and isotopic systematics of oceanic basalts: Implications for mantle composition and processes. In *Magmatism in the Ocean Basin*; Geological Society Special Publication: London, UK, 1989; Volume 42, pp. 313–345.
54. Nesbitt, H.; Young, G. Prediction of some weathering trends of plutonic and volcanic rocks based on thermodynamic and kinetic considerations. *Geochim. Cosmochim. Acta* **1984**, *48*, 1523–1534. [CrossRef]
55. Sanematsu, K.; Ejima, T.; Kon, Y.; Manaka, T.; Zaw, K.; Morita, S.; Seo, Y. Fractionation of rare-earth elements during magmatic differentiation and weathering of calc-alkaline granites in southern Myanmar. *Miner. Mag.* **2016**, *80*, 77–102. [CrossRef]
56. Wang, L.; Xu, C.; Zhao, Z.; Song, W.; Kynicky, J. Petrological and geochemical characteristics of Zhaibei granites in Nanling region, Southeast China: Implications for REE mineralization. *Ore Geol. Rev.* **2015**, *64*, 569–582. [CrossRef]
57. Chen, D.Q.; Wu, J.S. Mineralization mechanism of the ion-adsorption rare earth deposit. *J. Chin. Rare Earth Soc.* **1990**, *8*, 175–179.
58. Chen, Z.C.; Hong, H.H.; Zhuang, W.M.; Yu, S.J. A study on determination of rare earth species in weathering crust of granites. *J. Anal. Test.* **1993**, *4*, 21–25.
59. Wang, L.J.; Wang, Y.Q.; Zhang, S.; Liu, S.J.; Gao, X.J.; Sun, J.X.; Hu, A.T.; Chen, H.M.; Guo, F.Q. Speciation of rare earth elements in different types of soils in China. *J. Chin. Rare Earth Soc.* **1997**, *1*, 65–71.
60. Wood, S.A. The aqueous geochemistry of the rare-earth elements and yttrium: 1. Review of available low-temperature data for inorganic complexes and the inorganic REE speciation of natural waters. *Chem. Geol.* **1990**, *82*, 159–186. [CrossRef]
61. Wood, S.A. The aqueous geochemistry of the rare-earth element: Critical stability constants for complexes with simple carboxylic acids at 25 °C and 1 bar and their application to nuclear waste management. *Eng. Geol.* **1993**, *34*, 229–259. [CrossRef]
62. Yusoff, Z.M.; Ngwenya, B.T.; Parsons, I. Mobility and fractionation of REEs during deep weathering of geochemically contrasting granites in a tropical setting, Malaysia. *Chem. Geol.* **2013**, *349–350*, 71–86. [CrossRef]
63. Coppin, F.; Berger, G.; Bauer, A.; Castet, S.; Loubet, M. Sorption of lanthanides on smectite and kaolinite. *Chem. Geol.* **2002**, *182*, 57–68. [CrossRef]
64. Peng, X.; Wang, J.; Fan, B.; Luan, Z. Sorption of endrin to montmorillonite and kaolinite clays. *J. Hazard. Mater.* **2009**, *168*, 210–214. [CrossRef]
65. Huang, J.; He, H.; Tan, W.; Liang, X.; Ma, L.; Wang, Y.; Qin, X.; Zhu, J. Groundwater controls REE mineralisation in the regolith of South China. *Chem. Geol.* **2021**, *577*, 120295. [CrossRef]
66. Wu, Z.; Chen, Y.; Wang, Y.; Xu, Y.; Lin, Z.; Liang, X.; Cheng, H. Review of rare earth element (REE) adsorption on and desorption from clay minerals: Application to formation and mining of ion-adsorption REE deposits. *Ore Geol. Rev.* **2023**, *157*, 105446. [CrossRef]
67. Ichimura, K.; Sanematsu, K.; Kon, Y.; Takagi, T.; Murakami, T. REE redistributions during granite weathering: Implications for Ce anomaly as a proxy for paleoredox states. *Am. Miner.* **2020**, *105*, 848–859. [CrossRef]
68. Ohta, A.; Kagi, H.; Nomura, M.; Tsuno, H.; Kawabe, I. Coordination study of rare earth elements on Fe oxyhydroxide and Mn dioxides: Part I. Influence of a multi-electron excitation on EXAFS analyses of La, Pr, Nd, and Sm. *Am. Miner.* **2009**, *94*, 467–475. [CrossRef]
69. Quinn, K.A.; Byrne, R.H.; Schijf, J. Sorption of yttrium and rare earth elements by amorphous ferric hydroxide: Influence of pH and ionic strength. *Mar. Chem.* **2006**, *99*, 128–150. [CrossRef]

70. Chi, R.A.; Tian, J.; Luo, X.P.; Xu, Z.G.; He, Z.Y. The basic research on the weathered crust elution-deposited rare earth ores. *Nonferrous Met. Sci. Eng.* **2012**, *3*, 1–13.
71. Bau, M. Scavenging of dissolved yttrium and rare earths by precipitating iron oxyhydroxide: Experimental evidence for Ce oxidation, Y-Ho fractionation, and lanthanide tetrad effect. *Geochim. Cosmochim. Acta* **1999**, *63*, 67–77. [CrossRef]
72. Davranche, M.; Pourret, O.; Gruau, G.; Dia, A.; Jin, D.; Gaertner, D. Competitive binding of REE to humic acid and manganese oxide: Impact of reaction kinetics on development of cerium anomaly and REE adsorption. *Chem. Geol.* **2008**, *247*, 154–170. [CrossRef]
73. Xiao, S.; Liu, Y.; Zhao, W. Redox constraints on clay-sized rare earth element fractionation in weathered granite crust in the Chahe deposit, China. *Appl. Clay Sci.* **2024**, *254*, 107365. [CrossRef]
74. Cantrell, K.J.; Byrne, R.H. Rare earth element complexation by carbonate and oxalate ions. *Geochim. Cosmochim. Acta* **1987**, *51*, 597–605. [CrossRef]
75. Koeppenkastrop, D.; De Carlo, E.H. Sorption of rare-earth elements from seawater onto synthetic mineral particles: An experimental approach. *Chem. Geol.* **1992**, *95*, 251–263. [CrossRef]
76. Wu, P.Q.; Zhou, J.W.; Huang, J.; Lin, X.J.; Liang, X.L. Enrichment and fractionation of rare earth elements in ion-adsorption rare earth elements deposits: Constraints of iron oxide-clay mineral composites. *Geochemica* **2022**, *51*, 271–282.
77. Li, Y.H.M.; Zhou, M.F.; Williams-Jones, A.E. Controls on the Dynamics of Rare Earth Elements During Subtropical Hillslope Processes and Formation of Regolith-Hosted Deposits. *Econ. Geol.* **2020**, *115*, 1097–1118. [CrossRef]
78. Zhou, M.-F.; Li, M.Y.H.; Wang, Z.; Li, X.-C.; Liu, J. The genesis of regolith-hosted rare earth element and scandium deposits: Current understanding and outlook to future prospecting. *Chin. Sci. Bull.* **2020**, *65*, 3809–3824. [CrossRef]
79. Huang, Y.; He, H.; Liang, X.; Bao, Z.; Tan, W.; Ma, L.; Zhu, J.; Huang, J.; Wang, H. Characteristics and genesis of ion adsorption type REE deposits in the weathering crusts of metamorphic rocks in Ningdu, Ganzhou, China. *Ore Geol. Rev.* **2021**, *135*, 104173. [CrossRef]
80. Alshameri, A.; He, H.; Xin, C.; Zhu, J.; Xinghu, W.; Zhu, R.; Wang, H. Understanding the role of natural clay minerals as effective adsorbents and alternative source of rare earth elements: Adsorption operative parameters. *Hydrometallurgy* **2019**, *185*, 149–161. [CrossRef]
81. Gu, Q.; Liu, J.; Yang, Y.; Zhu, R.; Ma, L.; Liang, X.; Long, S.; Zhu, J.; He, H. The different effects of sulfate on the adsorption of REEs on kaolinite and ferrihydrite. *Appl. Clay Sci.* **2022**, *221*, 106468. [CrossRef]
82. Song, Y.H.; Shen, L.P. REE geochemistry of the weathering crust of acid volcanic rocks-An experimental study. *Geochimica* **1986**, *3*, 225–234.